The Deformation Vibrations of $[Os_{3-n}Ru_n(CO)_{12}]$ (n = 0—3) in the 150—30 cm^{-1} Region

By **Sidney F. A. Kettle,*** School of Chemical Sciences, University of East Anglia, Norwich NR4 7TJ
Pier Luigi Stanghellini, Istituto di Chimica Generale ed Inorganica, Universita di Torino, 10125 Torino, Italy

Although most models predict quite a large number of δ(CMM) and δ(CMC) bands for $[(MM')_3(CO)_{12}]$ systems only three strong bands are actually observed. This is explained in terms of a model in which the correlation of the local deformation modes with those of a ML_6 molecule of O_h symmetry plays a central role.

THEIR novelty and relevance to metal surfaces with catalytic properties have led to many recent studies of metal carbonyl cluster compounds. As far as the carbonyl ligands of such clusters are concerned, it has been found that for highly symmetric species, analyses of ν(CO) spectral features may be carried out in some detail.[1,2] In contrast, our understanding of the lower frequency regions is still very primitive, notwithstanding the fact that these regions are of particular relevance when attempting to relate metal cluster structures to metal surface geometries. We have elsewhere discussed the interpretation of the Raman spectra of $[M_3(CO)_{12}]$ (M = Os or Ru) species in the 200—150 cm^{-1} region.[3] In the present paper we are concerned with the region, 150—30 cm^{-1}, where δ(CMC) and δ(CMM) modes are expected to occur. The only previous work on these compounds in this spectral region is that of Quicksall and Spiro.[4]

EXPERIMENTAL

The syntheses of the complexes and the recording of the Raman spectra were performed as previously reported.[2]

RESULTS AND DISCUSSION

Quicksall and Spiro carried out a normal co-ordinate analysis of $[M_3(CO)_{12}]$ (M = Ru or Os) in the region 150—30 cm^{-1}, which assumed solely G-matrix coupling. The force constants obtained, although reasonable, were considerably constrained by the assumption that all Raman active modes would show some intensity and hence appear in the observed spectrum. In practice, this meant that all the Raman frequencies had to be placed in four narrow frequency regions, this being the number of bands Quicksall and Spiro reported [omitting the ν(M–M) bands which overlap with the upper end of the frequency range]. The spectra that we obtained for $[Os_{3-n}Ru_n(CO)_{12}]$ (n = 0—3) are shown in Figure 1(*a*)—(*d*). For n = 0 and 3 these spectra are essentially identical to those of Quicksall and Spiro except that the laser plasma emission lines in their spectra are absent (their spectrum of $[Ru_3(CO)_{12}]$ is marginally better resolved).

In $[Ru_3(CO)_{12}]$ the ν(M–M) modes appear at 187 (A_1') and 151 cm^{-1} (E') (A_1' is clearly the stronger). In $[Os_3(CO)_{12}]$ only this A_1' mode is clearly resolved, at 160 cm^{-1}. However, the 'δ(CMC)' peak at 119 cm^{-1} has become the strongest in this spectral region. We believe that this is because it contains both E' ν(M–M) and δ(CMC) features. It seems clear that this explanation is also true for $[Os_2Ru(CO)_{12}]$.[3] If these ν(M–M) peaks are deleted we find a close qualitative similarity between the spectra (*a*)—(*d*) in Figure 1, all have three strong peaks of comparable intensities at similar frequencies. Including all weak peaks which are apparent in the spectra (some of which have not been individually reported) there is a total of 12 for $[Ru_3(CO)_{12}]$, 11 for $[Os_3(CO)_{12}]$, and both $[Os_2Ru(CO)_{12}]$ and $[OsRu_2(CO)_{12}]$ show seven [excluding features assigned as ν(M–M)]. In contrast, an analysis based on the D_{3h} point group and ignoring site effects leads to a prediction of 10 Raman features (and more, of course, for the C_{2v} species). An analysis in D_{3h} supposes that the deformations about each metal atom are coupled together; were they not, an analysis based on the local C_{2v} symmetry at each metal atom would be appropriate. Such a C_{2v} analysis (Table 1) predicts eight Raman active features for the homometallic species and 16 for the hetero-. Details of the predictions of Table 1 are given in Table 2.

TABLE 1

Comparison of predicted and observed Raman spectra in the 150—30 cm^{-1} region [a]

Cluster	Predicted: molecular model D_{3h} (or C_{2v})	Predicted: local model C_{2v}	Observed [b]
$[Ru_3(CO)_{12}]$	10	8	12
$[OsRu_2(CO)_{12}]$	24	16	7
$[Os_2Ru(CO)_{12}]$	24	16	7
$[Os_3(CO)_{12}]$	10	8	11

[a] Although C_{2v} local symmetry is not strictly appropriate to all metal atoms in the heteronuclear clusters, the predicted number of peaks does not increase with a decrease in symmetry. [b] Excluding modes assigned as ν(M–M) but including weak features.

A possible explanation for the apparent observation of more Raman features in $[Ru_3(CO)_{12}]$ and $[Os_3(CO)_{12}]$ than predicted by the D_{3h} model is site symmetry splitting of degenerate modes. If this is so, such splitting should be yet more pronounced in the hetero-species for here it is molecular in origin. The observation that the hetero-species have the simplest spectra excludes this explanation. Alternatively, the additional features could have an anharmonic origin, possible involving lattice modes.

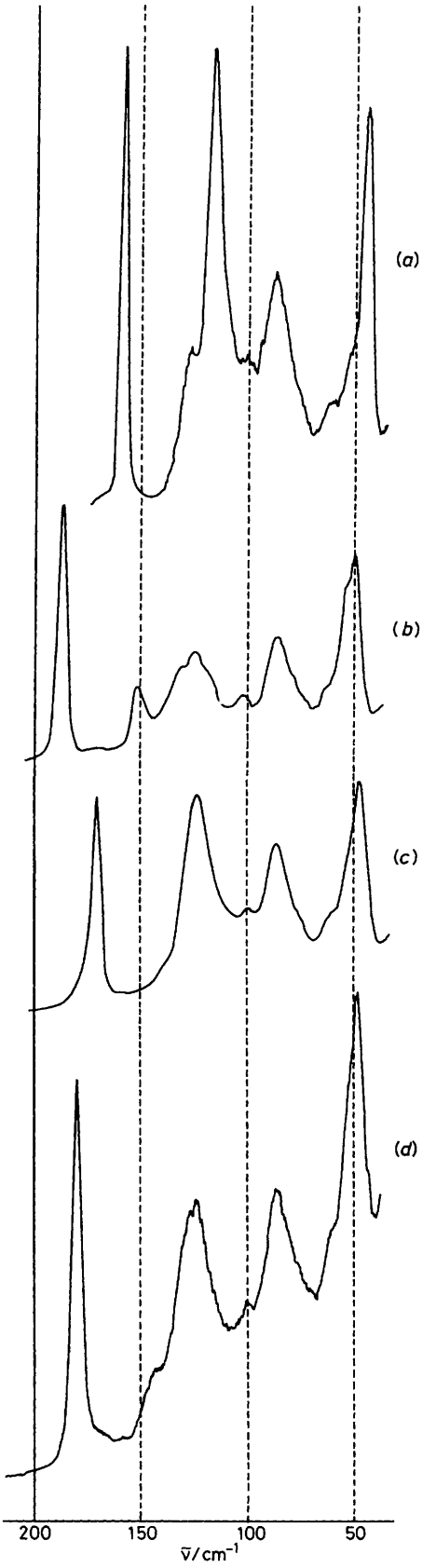

FIGURE 1 Raman spectra of: (*a*) $[Os_3(CO)_{12}]$; (*b*) $[Ru_3(CO)_{12}]$; (*c*) $[Os_2Ru(CO)_{12}]$; (*d*) $[OsRu_2(CO)_{12}]$, in the 30—150 cm^{-1} region

Because of the close similarity of $[Os_3(CO)_{12}]$ and $[Ru_3(CO)_{12}]$ [5] we would expect $[Os_2Ru(CO)_{12}]$ and $[OsRu_2(CO)_{12}]$ to be disordered on the lattice sites. Such disorder would lead to a broadening of lattice modes and, thus, to an apparently simpler spectra for the hetero-species; as observed.

We therefore conclude that the Raman spectra may be complicated by anharmonic features, a conclusion which places us in a difficult position. Which features are molecular in origin and which are not? We believe that the way out of this dilemma is provided by the comment made earlier that ' all (species) have three strong peaks of comparable intensities at similar frequencies.' We now present a model which rationalises this observation

TABLE 2

Alternative vibrational analyses of M_3C_{12} deformations

(*a*) D_{3h}

Number of vibrational modes = 39

ν(M–C)	$2A_1' + A_2' + 3E' + A_2'' + E''$
ν(M–M)	$A_1' + E'$
δ(CMC)	$2A_1' + A_2' + 3E' + A_1'' + A_2'' + 2E''$
$\delta(C_4–M_3)$	$A_2' + E' + A_1'' + A_2'' + 2E''$

The δ(CMC) and $\delta(C_4–M_3)$ modes are expected in the region below 150 cm^{-1} leading to a prediction of 10 Raman features ($2A_1' + 4E' + 4E''$)

(*b*) C_{2v}

We allocate two degrees of motional freedom to each C atom to give a representation $2A_1 + 2A_2 + 2B_1 + 2B_2$ and eight associated Raman features. The three pure rotations ($A_2 + B_1 + B_2$) correlate with $\delta(C_4–M_3)$ and the remainder with δ(CMC)

(*c*) *Correlations*

C_{2v}	D_{3h}
A_1	$A_1' + E'$
A_2	$A_1'' + E''$
B_1	$A_2' + E'$
B_2	$A_2'' + E''$

and *inter alia* provides an explanation for a limited number of additional features of molecular origin. The model is based on a local C_{2v} symmetry at each metal atom is therefore an additive one; the spectra of $[Os_2Ru(CO)_{12}]$ and $[OsRu_2(CO)_{12}]$ are regarded as superpositions of those of the homo-species with appropriate weightings.

The ' Distorted Octahedron ' Model.—The model we present is simple; it is based on the fact that the geometrical arrangement of the six atoms attached to a metal atom in a $[M_3(CO)_{12}]$ cluster is that of a distorted octahedron. In our model we correlate the deformations of a regular octahedron with those of the local C_{2v} symmetry at a metal atom in a $[M_3(CO)_{12}]$ cluster. That is, it is essentially the ' local C_{2v} model ' of Table 1 modified by intensity considerations.

The δ(LML) vibrations of an isolated octahedral ML_6 molecule provide a basis for $T_{1g} + T_{1u} + T_{2g} + T_{2u}$ irreducible representations of O_h; T_{1g} being, in our case, a near-redundancy (it corresponds to pure rotations in an ML_6 molecule). Of the others, only the T_{2g} has Raman activity in O_h. In the C_{2v} ocal metal environment encountered in $[M_3(CO)_{12}]$ the degeneracy of this T_{2g} set

will be totally removed (to give $A_1 + A_2 + B_1$ components). If the C_{2v} distortion is the dominant effect on these deformations, three Raman bands of comparable intensities will be observed, in qualitative accord with the experimental data. Whilst this agreement is the heart of our model it requires a more detailed analysis to sustain it and this we now present.

Because of our ignorance of the normal co-ordinates our analysis is both schematic and pictorial. In particular, we make extensive use of the symmetry co-ordinates shown in Figures 2 and 3. For convenience, we labelled these co-ordinates (*a*)—(*h*) (Figure 2) and (*j*)—(*s*) (Figure 3) and use these labels in the following

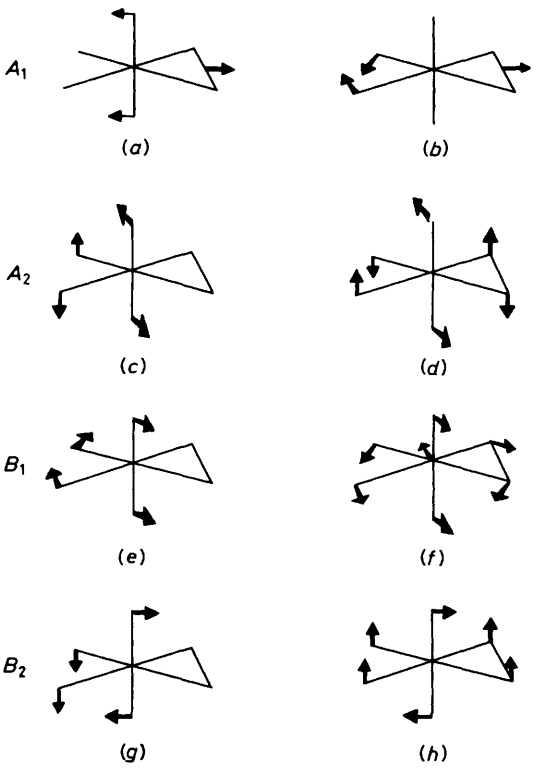

FIGURE 2 Schematic representations of the symmetry adapted combinations of C_4MM_2 deformations in C_{2v} symmetry. The M_3 plane is represented by a solid triangle and δ(MMM) ≡ ν(M–M) excluded; (*d*), (*f*), and (*h*) are δ(C_4–M_3); (*a*)—(*c*), (*e*), and (*g*) are δ(C–M–C)

discussion. Despite the schematic and pictorial nature of our analysis it is sufficient to ensure that the model provides a reasonable explanation of the experimental data.

The eight symmetry adapted combinations of the deformation modes in C_{2v} symmetry, labelled (*a*)—(*h*), are shown in Figure 2. In correlating these with the deformations of an ML_6 molecule, labelled (*j*)—(*s*) (Figure 3), we excluded the near-redundant T_{1g} rotations of the octahedron and, ultimately, the δ(MMM) mode, which is isomorphous to ν(M–M). These exclusions leave eight modes of the O_h model to be correlated with the eight of the C_{2v} model. In practice, however, it is easier to initially include δ(MMM) as an A_1 redundancy because this enables us to work with complete T_{1u}, T_{2g}, and T_{2u} sets in O_h. We note that it is only in the T_{1u} set that there is any motion of the central metal atom. The correlations between the vibrations shown in Figures 2 (C_{2v}) and 3 (O_h) are detailed in Table 3 where, for completeness, we have indicated possible minor T_{1g} contributions with an asterisk. One immediate conclusion emerges from Table 3. Excluding the A_1 redundancy in C_{2v}, it is clear that T_{2g} contributions will occur in a maximum of six δ(CMC) and δ(C_4–M_3) bands to first order in the C_{2v} model. This is in contrast to the simple group theoretical approach which also predicts B_1 activity and so two additional bands (see Table 1). The functions (*c*) and (*d*) of Figure 2 will have the approximate forms shown in equations (1) and (2) where (*p*) and (*q*) refer to

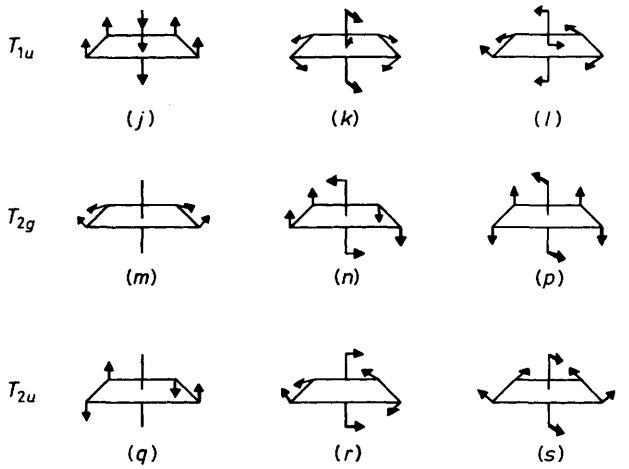

FIGURE 3 Schematic representations of the symmetry adapted combinations of ML_6 deformations on O_h symmetry. These representations differ from those commonly given because they are combinations correlating with C_{2v}

$$(c) = \sin\theta(p) + \cos\theta(q) \quad (1)$$

$$(d) = \cos\theta(p) - \sin\theta(q) \quad (2)$$

the orthogonal functions with these labels in Figure 3, ignoring any T_{1g} contribution. It follows that the relative T_{2g} contribution to the two A_2 (C_{2v}) modes derived from (*c*) and (*d*) will vary as $\sin^2\theta$ and $\cos^2\theta$. Contribution to the Raman activity of the A_2 modes originates in a single T_{2g} mode [labelled (*p*)]; the relative Raman intensities will vary as $\tan^2\theta$. It is sufficient to consider the range $0 \leqslant \theta \leqslant \frac{\pi}{2}$; for $\theta = \pi/4$ the bands will

TABLE 3

Correlations between the vibrations of Figures 2 and 3

C_{2v}/O_h	T_{1g}	T_{1u}	T_{2g}	T_{2u}
A_1 (*a*, *b*)		(*l*)	(*m*)	(*r*)
A_2 (*c*, *d*)	*		(*p*)	(*q*)
B_1 (*e*, *f*)	*	(*k*)		(*s*)
B_2 (*g*, *h*)	*	(*j*)	(*n*)	

Labels (*a*)—(*h*) refer to the modes illustrated in Figure 2 and (*j*)—(*s*) to those shown in Figure 3. An asterisk indicates possible minor T_{1g} contributions.

have equal intensities, while at $\theta = \pi/8$ and $3\pi/8$ the intensity ratio is 1 : 6. Entirely similar arguments apply to the B_2 (C_{2v}) modes derived from (*g*) and (*h*) where the intensity derives from the function labelled (*n*) in Figure 3.

For the $A_1(C)_{2v}$ modes the redundancy may be expressed in a simple form by equation (3) which is sufficiently accurate for the present argument; where (*m*), (*l*), and

$$\frac{1}{\sqrt{2}}\left[(m) - \frac{1}{\sqrt{2}}\{(l) + (r)\}\right] \quad (3)$$

(*r*) are the functions shown schematically in Figure 3. By forming the combination $\{(l) + (r)\}$ we annihilate any contribution from the deformations (represented by arrows in axial positions) in the diagrams representing (*l*) and (*r*) in Figure 3. The further combination with (*m*) annihilates any contribution from those deformations represented by arrows on the right hand side of diagrams (*l*), (*m*) and (*r*) of Figure 3. The above function therefore describes δ(MMM) — ν(M–M).

The two other A_1 modes must be orthogonal to this and to each other. That involving the maximum localization of Raman intensity is shown in equation (4) when

$$\frac{1}{\sqrt{2}}\left[(m) + \frac{1}{\sqrt{2}}\{(l) + (r)\}\right] \quad (4)$$

the third is given by equation (5). These latter two may, of course, be mixed. The key point is that some

$$\frac{1}{\sqrt{2}}\{(l) - (r)\} \quad (5)$$

significant Raman intensity goes with the redundancy; the ν(M–M) are strong in the Raman, so that we may expect a lower inherent A_1 intensity than either A_2 or B_2. This suggests that the peak at *ca.* 88 cm^{-1} in all of the spectra of Figure 1 should be assigned to this mode. Such an assignment is, incidentally, in agreement with that of Quicksall and Spiro, who predicted the A_1' and E' features (A_1-derived) (*cf.* Table 2) to occur within a few wavenumbers of each other in this region. However, by a similar argument their data predict the second set of A_1-derived features to be those at *ca.* 50 cm^{-1}. With this we disagree because of the strength of this band, although we do not exclude the possibility that the A_1-derived features are hidden beneath this strong band. We are unable to predict which of the bands at *ca.* 50 cm^{-1} and *ca.* 120 cm^{-1} is B_2 and which is A_2. In principle, infrared data could resolve this ambiguity because, as Table 3 shows, we would expect an i.r.–Raman correspondence for the B_2 feature. Unfortunately, the i.r. spectra show weak broad bands so that no useful information is immediately available.

Finally, if the arguments presented above are correct then they may be taken one step further. The comparability of intensity between the A_1, A_2, and B_2 features indicates that the A_1 functions discussed above are little mixed, but suggests that there is rather more mixing for A_2 and B_2. If this is so, weaker A_2 and B_2 features will be present in the spectra, *i.e.* there will be a total of five spectrally active bands in first order. The additional features seen could result from second order mixing between A_1 and B_1 modes (both correlate with molecular E' modes) and various forms of anharmonicities. As indicated earlier, there are suggestions that features involving lattice modes are seen in the spectra of the hetero-species.

We are indebted to the British Council, the C.N.R., and N.A.T.O. for financial support.

[1/932 *Received*, 10*th June*, 1981]

REFERENCES

[1] G. Bor, G. Sbrignadello, and F. Marcati, *J. Organomet. Chem.*, 1972, **46**, 357; G. Bor, G. Sbrignadello, and K. Noak, *Helv. Chim. Acta*, 1975, **58**, 815.

[2] G. B. Battiston, G. Bor, U. K. Dietler, S. F. A. Kettle, R. Rossetti, G. Sbrignadello, and P. L. Stanghellini, *Inorg. Chem.*, 1980, **19**, 1961.

[3] S. F. A. Kettle and P. L. Stanghellini, *Inorg. Chem.*, 1979, **18**, 2749.

[4] C. O. Quicksall and T. G. Spiro, *Inorg. Chem.*, 1968, **7**, 2365.

[5] M. R. Churchill and G. De Boer, *Inorg. Chem.*, 1977, **16**, 878; M. R. Churchill, F. J. Hollander, and J. P. Hutchinson, *ibid.*, p. 1655.